ACS APPLIED MATERIALS & INTERFACES

Research Article

www.acsami.org

Interfacial Properties of Organic Semiconductor–Inorganic Magnetic Oxide Hybrid Spintronic Systems Fabricated Using Pulsed Laser Deposition

Sayani Majumdar,[*,†] Katarzyna Grochowska,[‡] Miroslaw Sawczak,[‡] Gerard Śliwiński,[‡] Hannu Huhtinen,[§] Johnny Dahl,[⊗] Marjukka Tuominen,[⊗] Pekka Laukkanen,[⊗] and Himadri S. Majumdar[⊥]

[†]Department of Applied Physics, Aalto University School of Science, FI-00076 Aalto, Finland

[‡]Photophysics Department, The Szewalski Institute, Polish Academy of Sciences, 80-231 Gdansk, Poland

[§]Wihuri Physical Laboratory, Department of Physics and Astronomy, University of Turku, FI-20014 Turku, Finland

[⊗]Materials Research Laboratory, Department of Physics and Astronomy, University of Turku, FI-20014 Turku, Finland

[⊥]VTT Technical Research Center of Finland, FI-02150 Espoo, Finland

ABSTRACT: We report fabrication of a hybrid organic semiconductor–inorganic complex oxide interface of rubrene and $La_{0.67}Sr_{0.33}MnO_3$ (LSMO) for spintronic devices using pulsed laser deposition (PLD) and investigate the interface structure and chemical bonding-dependent magnetic properties. Our results demonstrate that with proper control of growth parameters, thin films of organic semiconductor rubrene can be deposited without any damage to the molecular structure. Rubrene, a widely used organic semiconductor with high charge-carrier mobility and spin diffusion length, when grown as thin films on amorphous and crystalline substrates such as SiO_2-glass, indium–tin oxide (ITO), and LSMO by PLD at room temperature and a laser fluence of 0.19 J/cm^2, reveals amorphous structure. The Raman spectra verify the signatures of both A_g and B_g Raman active modes of rubrene molecules. X-ray reflectivity measurements indicate a well-defined interface formation between surface-treated LSMO and rubrene, whereas X-ray photoelectron spectra indicate the signature of hybridization of the electronic states at this interface. Magnetic measurements show that the ferromagnetic property of the rubrene–LSMO interface improves by >230% compared to the pristine LSMO surface due to this proposed hybridization. Intentional disruption of the direct contact between LSMO and rubrene by insertion of a dielectric AlO_x layer results in an observably decreased ferromagnetism. These experimental results demonstrate that by controlling the interface formation between organic semiconductor and half-metallic oxide thin films, it is possible to engineer the interface spin polarization properties. Results also confirm that by using PLD for consecutive growth of different layers, contamination-free interfaces can be obtained, and this finding is significant for the well-controlled and reproducible design of spin-polarized interfaces for future hybrid spintronics devices.

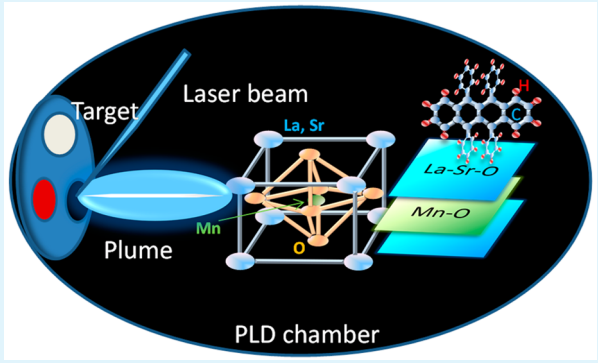

KEYWORDS: *pulsed laser deposition, organic spintronics, organic semiconductor thin films, magnetic properties, hybrid interface*

INTRODUCTION

Hybrid electronics is the future of electronics, and proper understanding of the interface between the hybrid components is key to the development of this field. For the nanomagnetism and spintronics community, the interface between inorganic ferromagnets and organic semiconductors is an area of major research interest due to the possibility of incorporating the best potential materials for optimally functional devices.[1−4] For spintronic components the inorganic ferromagnetic (FM) functional oxides and organic semiconductor (OS) small molecules and polymers form a promising combination as inorganic complex oxides show nearly 100% spin polarization[5] and organic compounds are supposed to have very long spin relaxation length and time due to their smaller spin–orbit and hyperfine coupling arising from the light constituent atoms such as C, H, and N.[6] During the first decade of the development of "organic spintronics", many successes were reported including spin injection[7] and transport[1] in low-mobility OS molecules, sizable giant and tunneling magneto-resistance effects (GMR and TMR, respectively) in organic spin valves and magnetic tunnel junctions, and measurement of sizable spin diffusion length and time in OS small molecules[8] and polymers.[9] However, with the rapid advancement of the field, more and more challenges also started to appear. One

Received: June 2, 2015
Accepted: September 24, 2015
Published: September 24, 2015

DOI: 10.1021/acsami.5b04840
ACS Appl. Mater. Interfaces 2015, 7, 22228−22237

such challenge is temperature-dependent spin relaxation length in OS small molecules and polymers,[7,10] which leads to negligible GMR response from the spin valve devices at room temperature. Also, the absence of a Hanle effect in organic semiconductor-based spintronic components raised a debate about spin injection through organics; however, it is also not clear whether the Hanle effect can be expected in a system where spin transport is mainly through incoherent hopping transport.[11]

Another important concern for the research community is to understand and control the FM/OS interface designed for functional devices. It has been recently reported by several groups that *p-d* hybridization and charge transfer reaction at the interface can significantly modify the spin polarization property.[12,13] It was also shown that *p-d* hybridization and charge transfer strongly depend on the position and orientation of the aromatic molecule surface on the ferromagnetic interface.[14] Therefore, the atomic level control over the growth of OS on the FM surface and the hybrid interface can significantly modify and improve the performance of this spintronic devices. However, for precise control over the *p-d* hybridization at the interface, it is essential to measure and control the purity of the interface with minimum defects. Fabricating a clean and well-defined interface between the magnetic oxides and the organics is a challenging task because the fabrication process of hybrid devices often involves the use of different deposition methods for oxides and organic materials. The ferromagnetic oxides require high-temperature growth in a controlled oxygen atmosphere, whereas organic materials require evaporation or spin coating in a vacuum or inert environment. Therefore, the device fabrication process needs transfer of samples between the chambers for inorganic and organic thin film depositions. Transferring samples under ultrahigh vacuum (UHV) (10^{-9} mbar) conditions is an option for maintaining the purity of the interface; however, under UHV conditions, oxides such as LSMO can lose oxygen from the surface, which can significantly modify its surface magnetic properties. Also, many laboratories do not have UHV facilities for sample transfer, and in many cases sample transfer is done by breaking the high-vacuum condition between the two deposition steps. This contaminates the interface with environmental carbon, oxygen, and other impurities during sample handling, and this unintentional contamination of the device interfaces can consequently cause significant variation in the device properties. It has been also shown experimentally that introduction of this contamination changes the interface energetics significantly.[15]

Within the framework of the present study, we explored the possibility of growing an OS, which is of interest for spintronic applications, in a way different from the traditional routes to improve control over the interface properties and minimize the contamination effects. PLD is a versatile technique for stoichiometric deposition of materials in a controlled way in clean conditions and is generally used for inorganic metals and oxides.[16,17] As the high energy of the laser pulses can destroy the soft organic molecules, this technique has not been popularly used for deposition of organic semiconductors. In this work PLD has been used to grow the thin film of rubrene ($C_{42}H_{28}$), a widely used OS material for transistors with reasonably good charge carrier mobility and spin diffusion length.[6] Although a literature review shows only a few papers on the growth of organic semiconductors such as pentacene[18,19] and a few different polymers[20] using PLD, the report of back-to-back fabrication of complex metal oxides and soft organic materials using the same PLD, or other fabrication methods, is missing. The possibility of using the same method to deposit both types of materials provides an opportunity to fabricate atomically clean device interfaces and simplifies the device fabrication process for future industrial applications. The PLD technique requires optimized parameters for growth of thin films with identical structural and electronic properties as the bulk target material. Also, the possibility of engineering materials at the nanoscale by varying the laser fluence, substrate temperature, deposition rate, annealing, etc., offers the opportunity for modified structure and functionality. For organic materials, using the pulsed laser requires careful control as high-energy laser pulses can destroy the molecular structure. The literature shows that a high-quality *c** axis oriented pentacene film can be grown using PLD with significant improvement in device performance when the proper growth[21] and annealing conditions are applied.[22] Salih et al. showed that among different parameters, laser wavelength and fluence determine the properties of the films.[23] In the present work, rubrene, a well-studied organic small molecule without any heavy elements in its structure and consequently promising charge and spin transport properties, has been chosen to test whether it is possible to grow more crystalline phases using similar PLD parameters. The success of the process could lead to better control of crystallinity and hence carrier mobility and spin diffusion lengths of OS.

In this work, we have developed and optimized the PLD growth process of rubrene molecules[24] and systematically studied the effect of removal of contaminations at the FM/OS interface by studying the structural, electronic, and magnetic properties. For this purpose, rubrene films were grown on $La_{0.67}Sr_{0.33}MnO_3$ (LSMO), a well-known half-metallic manganite.[25] Although manganites are not considered as industrially viable materials, the choice of manganites in the current context was made to investigate a proof of concept system where controlled interface formation between a magnetic oxide and an organic semiconductor can be studied for understanding the spin engineering phenomenon at the interface. This result could be tested in the future for other half-metallic oxides such as Fe_3O_4 and CrO_2 that could be useful for industrial application. The LSMO/OS interface was modified by different conditions such as high temperature in situ annealing before OS deposition and by insertion of the dielectric AlO_x layer. High-temperature (500 °C) annealing of LSMO was performed under vacuum conditions (10^{-6} mbar) to reduce contamination on the surface of the LSMO film and hence at the hybrid interface, as previously reported by Grobosch et al.[15] The effect of removal of contamination and insertion of a seed layer on the structural and magnetic properties of the LSMO/rubrene interface were then thoroughly studied, and this knowledge could consequently lead to improved control of the device properties.

EXPERIMENTAL SECTION

The rubrene target for the PLD process was prepared in the form of a pellet from commercially available powder (Sigma-Aldrich, purity ≥ 98%) and annealed to the melting point (315 °C) in an inert atmosphere. The PLD process was carried out in vacuum conditions (5×10^{-6} mbar) at room temperature. The radiation of a Nd:YAG laser (Quantel) operating at 1064 nm, 6 ns pulse duration, and 2 Hz pulse repetition was focused on the target surface using quartz lens. The pulsed laser energy for organic layer deposition was chosen on the basis of the literature value,[26] which showed that it is safe to grow

DOI: 10.1021/acsami.5b04840
ACS Appl. Mater. Interfaces 2015, 7, 22228−22237

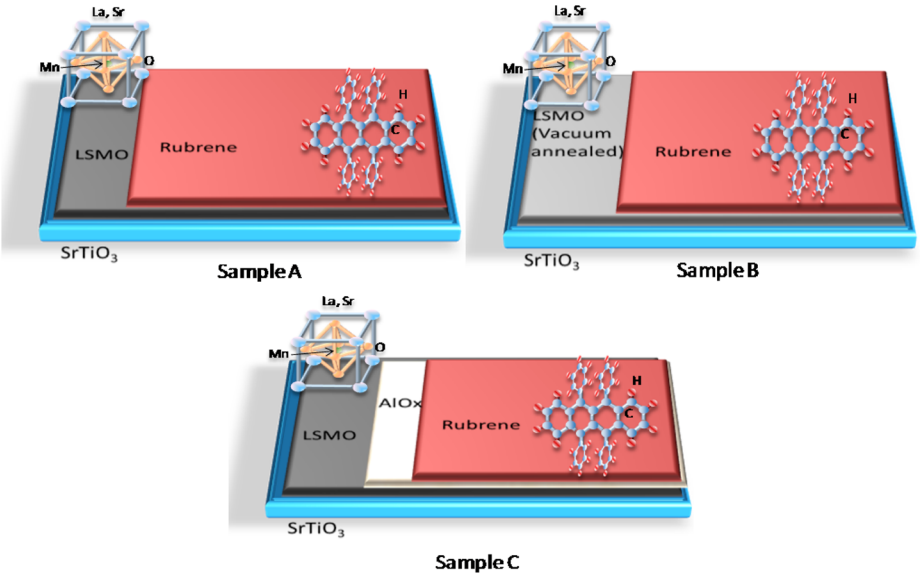

Figure 1. Schematic diagram of the architectures of the grown multilayers with LSMO crystal structure and chemical structure of the rubrene molecule.

Table 1. Description of the Samples Together with Characteristic Physical Parameters: Surface Roughness, RMS Value, Saturation Magnetization M_S, Curie Temperature T_C, Coercive Field H_C, and Relative Change in Magnetization Due to Modified Interface $\Delta M/M$

sample	description	RMS roughness (nm)	M_S at 5K (10^5 A/m)	T_C (K)	H_C at 5K (mT)	$\Delta M/M$ at 5K (%)
LSMO	as grown 20 nm	0.5	4.66	322.7	0.5	0
A	rubrene (8 nm)/LSMO(20 nm)	2.0	4.85	333.4	1.5	4.2
B	rubrene (8 nm)/vac-treated LSMO (20 nm)	1.2	4.48	319.8	2.5	−3.8
C	rubrene (8 nm)/AlO_x(1−2 nm)/LSMO (20 nm)	1.0	4.07	319.8	2.5	−12.8

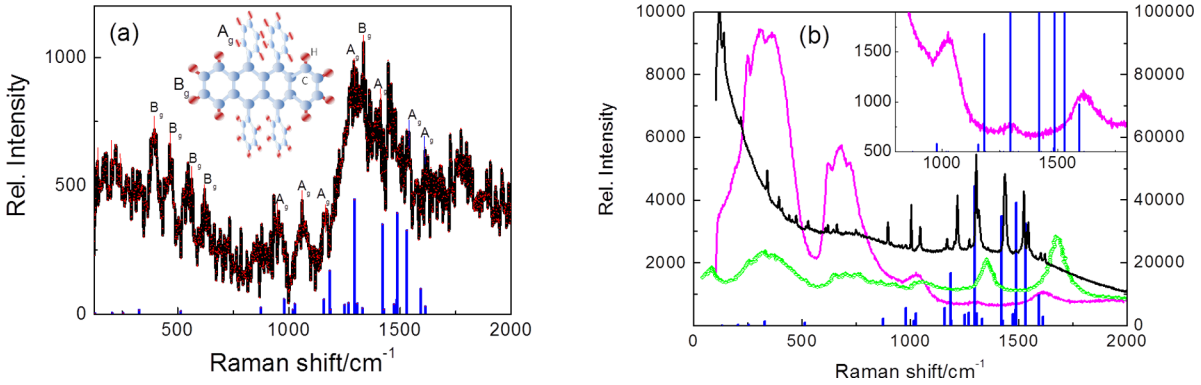

Figure 2. (a) Raman spectrum of rubrene thin film on glass at room temperature taken with excitation at 785 nm together with reported Raman active frequencies from ref 28 (blue lines); (b) same spectra for rubrene on LSMO/STO (purple line) together with Raman active modes of the rubrene powder (black line) and STO substrate (green line) for reference.

organic thin films within the laser fluence range of 0.06−0.9 J/cm^2. For the rubrene deposition the laser fluence was established at the level of 0.19 J/cm^2 to produce a growth rate of up to 0.26 nm/min. In the case of AlO_x deposition, the growth rate at the level of 1 nm/min for laser fluence of 0.8 J/cm^2 was measured. Details of the rubrene deposition have been reported elsewhere.[24]

Initially, the rubrene films were grown on SiO_2 glass substrates, and the profilometric inspection was performed for calibrating the thickness and for further understanding of the deposition parameters. To check the molecular structure of the deposited rubrene, the Raman spectra of the films were measured using the micro-Raman spectrometer (InVia, Renishaw) operating with 785 nm excitation. Atomic force microscopy (AFM), X-ray reflectivity (XRR), and X-ray photoelectron spectroscopy (XPS) measurements were also performed to characterize the surface morphology, interface roughness, and chemical structure of the grown films. AFM was done using a microscope model 5000 (Veeco Dim.) operating in tapping mode, and the XRD and XRR characterization was performed using the spectrometer X'Pert (Panalytical) with Cu Kα radiation. XPS spectra were measured using a PerkinElmer PHI 5400 spectrometer with a monochromatized Al Kα X-ray source operating at 14 keV and an analyzer pass energy of 18 eV. For transport measurements, the growth of rubrene films of thicknesses of 42 and 56 nm on the etched ITO-coated glass substrates was followed by deposition of the Al top electrodes (ITO/rubrene/Al sandwich structure), and the I−V characteristics were measured using a Keithley semiconductor analyzer. After the structural and transport properties of the grown rubrene samples had been verified, several rubrene samples were

DOI: 10.1021/acsami.5b04840
ACS Appl. Mater. Interfaces 2015, 7, 22228−22237

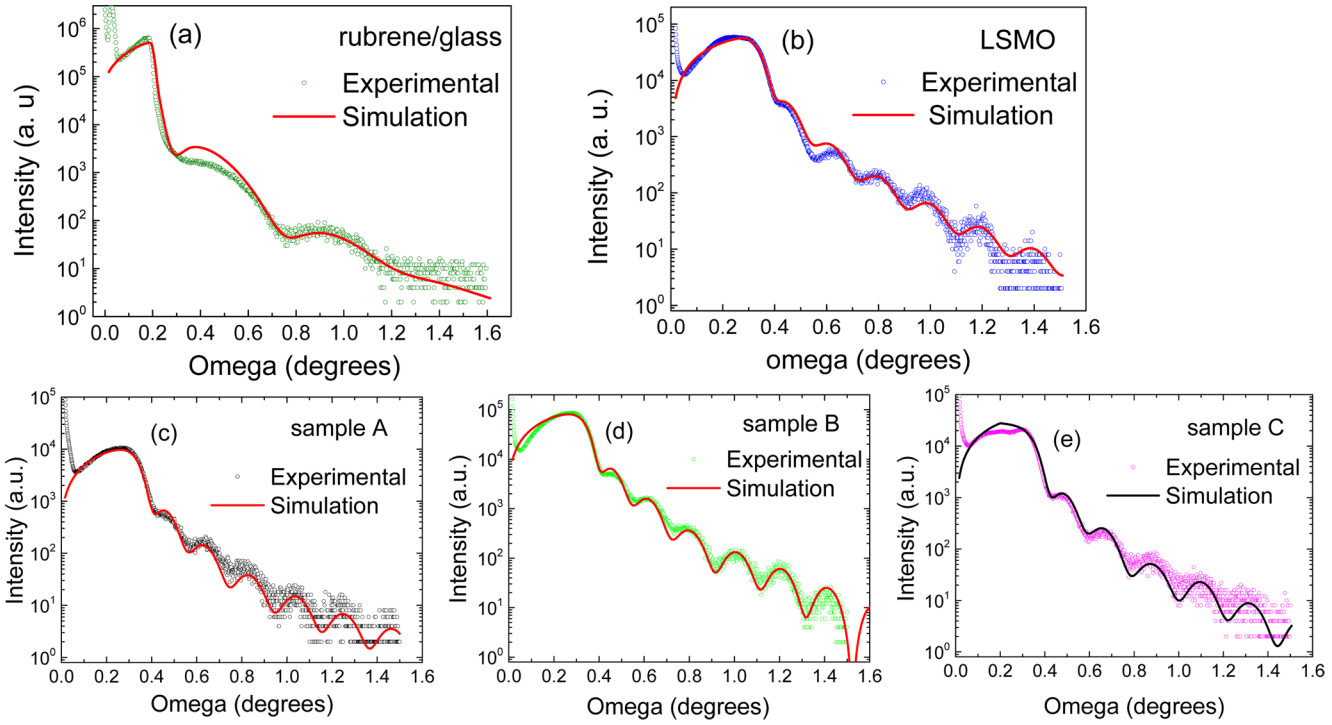

Figure 3. XRR patterns of the (a) rubrene thin film on glass and (b) LSMO film on STO (open circles) and of (c) sample A, (d) sample B, and (e) sample C, together with model fitting (solid lines).

deposited on LSMO. The 20 nm thick LSMO films were previously grown on $SrTiO_3$ (STO) (001) substrates using the procedure reported elsewhere.[27] The 8 nm thick rubrene film on as-grown LSMO was deposited using identical parameters as mentioned above and named sample A. Next, vacuum annealing at 500 °C was done on LSMO to remove the carbon contamination on the LSMO surface, and then rubrene of similar thickness was deposited and named sample B. The sample prepared with a 1−2 nm aluminum oxide (AlO_x) film between the LSMO (as-grown) and the rubrene layers was named sample C. The schematic of the device architectures, together with the crystal structure of LSMO and chemical structure of rubrene molecule, is shown in Figure 1. Magnetization measurements as a function of temperature (*M*-*T*) and magnetic field (*M*-*B*) were conducted using a SQUID-MPMS (Quantum Design) magnetometer on all of the above-mentioned samples together with sample A after its rubrene layer had been cleaned with acetone and alcohol (sample D). To avoid the issue of reproducibility of magnetic properties among different LSMO films, all the rubrene samples were grown on 5 × 5 mm^2 pieces cut from one single 10 × 10 mm^2 LSMO film. Description of the samples and their important parameters are summarized in Table 1.

RESULTS AND DISCUSSION

Structural Properties. Profilometry confirmed continuous growth of the 8 nm rubrene film on SiO_2, and the AFM characterization in tapping mode showed complete coverage of rubrene film on glass and growth of a relatively smooth surface without scattered island formation.[24]

Raman spectra of the 8 nm rubrene film on SiO_2, although dominated by the fluorescence, showed the signature of Raman active modes (Figure 2, left panel) of the rubrene molecule reported in the literature.[28] This molecule consists of a tetracene backbone and four phenyl side groups, where the tetracene backbone of the rubrene molecule is planar. In Raman spectra the tetracene core is represented as B_g mode, whereas the phenyl groups are shown by the A_g mode. The presence of both B_g and A_g modes in the Raman spectra and the broad band at 1373 cm^{-1} verifies the growth of amorphous rubrene thin films. For the rubrene film on LSMO, the spectrum is dominated by Raman active modes of STO single-crystal substrate, making observation of the Raman signal from thin rubrene films and LSMO challenging. This is understandable due to much larger thickness of the STO substrate (500 μm) compared to LSMO (i.e., 20 nm) and rubrene (8 nm). However, small bands near 1000 and 1500 cm^{-1} could be linked to the Raman signal of the rubrene molecules.

The structural properties of rubrene films were also investigated by means of the XRR, XRD, and XPS techniques. The thickness of the individual layers, the surface and interface roughnesses, and the average density of the system of the rubrene thin film, LSMO, and samples A, B, and C were calculated from XRR data and model fitting (Figure 3). For rubrene, the XRR curves confirm that the grown films are continuous, with densities close to the reported values[29] and smooth surfaces. Calculation of the average roughness of rubrene on glass gives a value of 1.3 nm and a thickness of 8.5 nm of the grown layer, in agreement with the thickness value shown by the profilometer. The mass densities of the films grown on glass substrates are 1.22 g/cm^3, which is quite close to the reported value of 1.26 g/cm^3.[27] For the single-layer LSMO, the surface roughness is 0.5 nm for a 20 nm film, and the mass density is 6.2 g/cm^3.

For rubrene on LSMO, the reflectivity signals from the samples are dominated by that of LSMO due to higher atomic weight of LSMO compared to rubrene. However, the critical angle (below which total reflection occurs) reduces in comparison to LSMO, suggesting a combined signal from both higher and lower density materials. Another noticeable feature is the improved oscillation with lesser slope for sample B compared to samples A and C. This indicates that due to vacuum annealing treatment before the rubrene deposition, the interface between LSMO and rubrene becomes better defined and the roughness at the interface of LSMO and rubrene

DOI: 10.1021/acsami.5b04840
ACS Appl. Mater. Interfaces 2015, 7, 22228−22237

decreases. Although simulation of parameters from an XRR pattern of a multilayer is dependent on many factors, the improved roughness values of rubrene layer on samples B (1.2 nm) and C (1 nm) compared to sample A (2.0 nm) are consistently observed. This confirms the improved growth conditions of the rubrene layer due to vacuum annealing and inclusion of an AlO_x layer. Growth of better quality rubrene on an AlO_x seed layer was also reported previously by the Moodera group.[6]

X-ray diffraction of rubrene powder generally shows orthorhombic crystal structure; however, the XRD spectra of the thin films (8 and 44 nm) showed no peaks from rubrene on glass, indicating growth of amorphous phase in agreement with Raman measurements. This indicates that the growth of crystalline rubrene phase will require additional thermal treatment or modified PLD growth conditions of the films.

Electronic Properties of the FM/OS Interface. XPS is a powerful technique for understanding the interface chemistry and the energy level alignments in organic/inorganic-based devices. To study the electronic properties at the LSMO/rubrene interface, XPS measurements were performed on all of the samples. Figure 4 shows O 1s and C 1s spectra from these

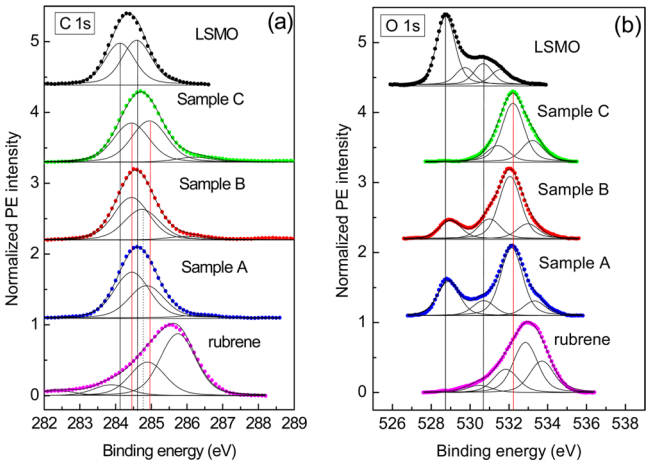

Figure 4. X-ray photoelectron spectroscopy of (a) C 1s and (b) O 1s core levels for pure LSMO and rubrene samples together with the LSMO coated with rubrene (as grown, surface treated, and one with an AlO_x layer in between).

five chosen samples without any specific surface treatments. The pure rubrene sample showed a significant charging effect, which caused a shift of the C 1s peak to the higher binding energy side. In the recorded spectra, this charging effect has been compensated by taking the SiO_2 peak as reference. It follows from the figure that the C 1s core level peak of rubrene can be fitted with four components, which in turn can be attributed to the pure aromatic carbon (C—C) (282 eV), C═C (283.8 eV), and C—OH or C—O (286 eV) bonding sites. The literature shows that pure rubrene depicts only the aromatic carbon peak and the peaks O 1s are not revealed. Therefore, our core level spectra indicate that the top layer of the rubrene film is oxidized due to exposure to atmosphere. For the LSMO, the C 1s peak constituted of two components C—C (284.1 eV) and C—O—C (284.6 eV) is mainly due to atmospheric C as the pristine sample does not contain any C. For samples A, B, and C, three contributions of the C 1s spectra are present corresponding to the atmospheric C, aromatic C, and hydroxyls of C. Compared to samples A and B, the aromatic carbon peak in sample C is shifted toward the higher binding energy (BE) side by 0.1 eV. This indicates that the growth of rubrene is quite different on AlO_x compared to that on LSMO. Also, whereas sample A reveals the aromatic C peak almost at the same location as the pristine rubrene sample, this peak for sample B shows a shift toward lower BE by 0.09 eV. Therefore, it can be concluded that the lower BE peak (284.47 eV) is due to atmospheric carbon and the higher BE peak corresponds to aromatic carbon of rubrene. The shift of this peak observed for three differently grown samples indicates that due to modified LSMO surface and hence LSMO/rubrene interface, the electronic bonding of rubrene molecules becomes affected. Compared to samples A and B, the carbon peak is broadened to the higher BE, indicating that the growth of rubrene is quite different on AlO_x compared to that on LSMO.

For the pristine LSMO, the O 1s peak around 528 eV is observed with a little shoulder on the higher BE side at 530 eV. This high-energy shoulder is most probably caused by surface contaminants (the surface was not treated before XPS), which is consistent with the appearance of the C 1s emission. The surface contamination may be the result of physisorbed, chemisorbed, and structural H_2O together with hydroxide (OH−) and CO_2 contributions.[30] Both the rubrene single layer and the samples on LSMO also showed oxygen peak due to atmospheric oxygen (~532 eV). For samples A and B, both the peaks from LSMO O 1s and atmospheric oxygen are observed without any significant shift in the BE value. The O 1s peak of pure rubrene film can be fitted using four curves corresponding to C═O, C—O, C—O—C, and O—C═O bonding environments from lower to higher BE, respectively. Samples on LSMO, however, show better fitting with three components corresponding to C—O, C—O—C, and O—C═O. The lower BE peak of O 1s becomes suppressed for sample B of the surface treatment performed before rubrene deposition, which indicates a decreased oxygen level in this sample. For sample C the LSMO peak O 1s could not be measured due to the presence of an additional AlO_x layer.

The Mn $2p_{3/2}$ core level spectra of LSMO reveal peaks at 642 and 654 eV, and both of these peaks can be fitted using three different components as shown in Figure 5a. A possible explanation for these components could arise from the fact that

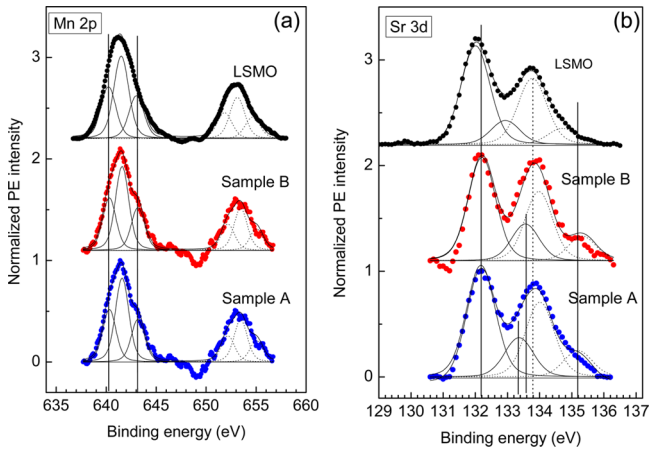

Figure 5. XPS core level spectra of (a) Mn 2p and (b) Sr 3d for pure LSMO and rubrene samples together with the LSMO coated with rubrene (as grown, surface treated, and one with an AlO_x layer in between).

DOI: 10.1021/acsami.5b04840
ACS Appl. Mater. Interfaces 2015, 7, 22228−22237

two of them of the lower BE are due to the exchange interaction between the core holes and the valence electrons. In this picture, the high- and low-BE components correspond to the majority and minority of spin core−hole states, respectively, and the energy separation between them, Δ_{ex}, corresponds to the exchange splitting of the Mn 2p core−hole states.[31] Due to deposition of rubrene (in both samples A and B), a shoulder structure starts to appear at the higher BE side of both peaks (at 655 eV). This shoulder structure is previously interpreted as the well-screened peak of the Mn^{3+} state, and its intensity is considered to represent the metallicity of the system.[32] However, between the as-grown and surface-treated samples, no significant changes in the Mn 3d core states can be observed.

For the Sr 3d core-level spectra of LSMO (Figure 5b), however, surface treatment before rubrene deposition made a significant difference in the peak intensity and binding energies, mainly in the higher BE peak.

The Sr 3d spectra of LSMO show splitting of the Sr peak into $3d_{3/2}$ to $3d_{5/2}$ components. Whereas the observed spin−orbit splitting of about 1.8 eV is expected, it can be observed that the interface-related Sr component, that is, the small-intensity solid line peak around 133.4 eV, is shifted as compared to the pure LSMO. This shift to the high BE side reflects a rubrene-induced interface effect, which leads to a decrease of the electronic potential around the interface Sr atoms at the rubrene interface, as compared to the pure Sr. The line shapes of both Mn 2p and Sr 3d spectra change substantially due to the growth of rubrene, indicating that the hybrid interface formation results in a change of the electronic environments around the Mn and Sr ions. Larger differences in the Sr 3d peaks between as-grown and surface-treated LSMO sample thus clearly indicate that the La−Sr−O plane is the terminating layer of LSMO and becomes more modified due to rubrene deposition compared to the Mn−O plane (as shown in Figure 6). However, a small change in the Mn 2p line shape also indicates that some rubrene molecules penetrate the surface layer and modify the Mn electronic environment as well.

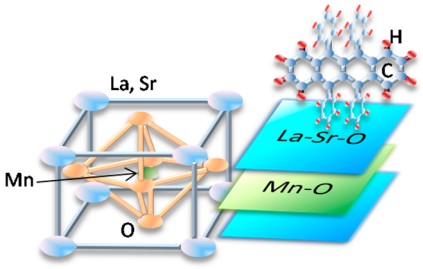

Figure 6. Schematic interpretation of the interface electronic structure between LSMO and rubrene molecules.

Transport Properties of ITO/Rubrene/Al Diodes. To check if the grown OS layer reveals the charge-transport ability required for spintronics application, the test ITO/rubrene (42 nm)/Al device structure (details given under Experimental Section) has been produced under identical deposition condition as sample A. The measured I−V characteristic is shown in Figure 7. It reveals nonlinear behavior with a little asymmetry for the positive and negative applied bias. Also, depending on the thickness of the rubrene layer, the device currents change (not shown here), which indicates that charge

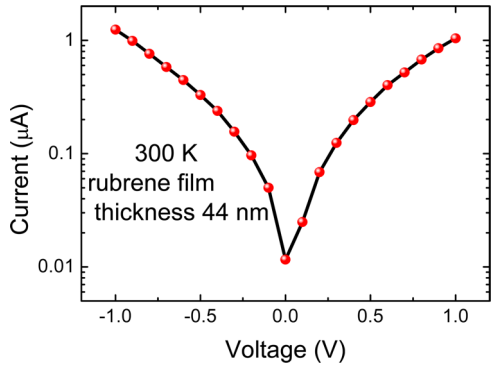

Figure 7. I−V characteristics of the ITO/rubrene/Al diode device at room temperature showing nonlinear, asymmetric nature.

transport takes place via a hopping mechanism through the deposited rubrene layer and not through metallic pinholes.

To confirm this conclusion, the charge carrier mobility was calculated for the deposited rubrene layer using the relationship $\sigma = ne\mu$, where σ, n, and μ are the conductivity, charge carrier density, and carrier mobility, respectively. Calculating σ from the I−V data at 1 V, and using the carrier density value from the literature,[33] carrier mobility of the order of 10^{-6} $cm^2/(V\ s)$ was estimated, which is in good agreement with the experimentally obtained mobility values for amorphous rubrene.[34] The result again confirms that the grown rubrene layer is amorphous with randomness in intermolecular separation leading to the formation of defects and grain boundaries that could trap charge carriers. However, sizable current through the device is an indication that charge and spin polarized carriers can pass through this layer by hopping for thick layers or by multistep tunneling via localized states for the thinner rubrene layer. An increase in the crystalline order can be expected with further control of the growth parameters and could lead to higher carrier mobility and spin diffusion length, too.

Magnetic Properties of FM/OS Interfaces. For investigation of the magnetic properties and hence the spin polarization of the hybrid interfaces, detailed temperature (*M-T*) and field dependent (*M-B*) magnetization measurements were carried out on the samples. Results indicate that paramagnetic (PM) to FM phase transition starts similarly in all samples, but eventually in the FM phase there are distinct differences in the magnetic moment values. The saturation magnetic moment (M_S) value of the pristine LSMO film is 5.135 μ_B/formula unit (fu), which is higher than the theoretically calculated value of 4.657 μ_B/fu for 33% hole-doped LSMO (using the Mn^{3+} moment of 5 μ_B/fu and the Mn^{4+} moment of 3.9 μ_B/fu for octahedral co-ordination), indicating the good quality of the deposited LSMO films. The *M-T* data indicate improvement of the ferromagnetic properties of LSMO due to the presence of the rubrene. The M_S value increases from 5.135 to 5.819 μ_B/fu, and the Curie temperature (T_C) increases from 322.8 to 333.4 K, as shown in Figure 8a,b in the case of rubrene deposited directly on LSMO. This improved ferromagnetism due to organic coating can be attributed either to the prevention of dangling oxygen bonds, which often are observed at the surface of the film as result of abrupt termination of the MnO_6 octahedra,[35] or to the proposed hybridization process that allows a charge-transfer mechanism between aromatic molecules and ferromagnetic oxide, consequently improving ferromagnetism.[36] Also, there

DOI: 10.1021/acsami.5b04840
ACS Appl. Mater. Interfaces 2015, 7, 22228−22237

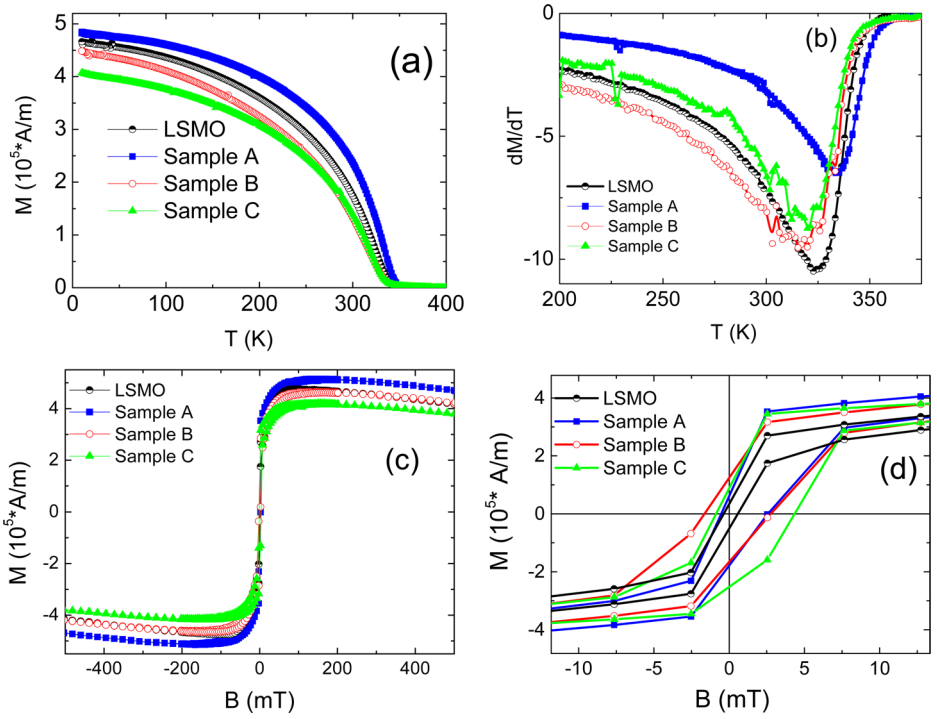

Figure 8. Field-cooled (FC) magnetization as a function of (a) temperature and (c, d) magnetic fields together with the first derivative of magnetization (b) for pure LSMO and the LSMO coated with rubrene (as grown, surface treated, and one with an AlO_x layer in between).

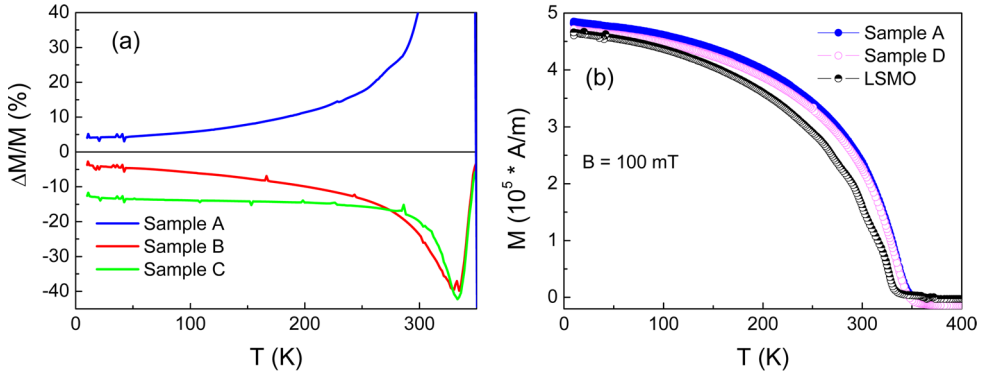

Figure 9. (a) Relative change in magnetization ($\Delta M/M$) as a function of temperature for sample A, B, and C together with (b) M versus T for pure, rubrene-coated (sample A), and sample from which the rubrene layer has been removed (sample D).

could be effects from an induced moment on rubrene due to close contact with a ferromagnetic electrode. More on this will be discussed later. Due to the surface treatments done with high-temperature vacuum annealing, the magnetic properties of the ferromagnetic/organic interface become suppressed compared to sample A and the bare LSMO. This can be attributed to the loss of oxygen at the LSMO surface at high temperature, leading to a surface with oxygen vacancy related defects. Also, loss of oxygen causes reduction of Mn^{4+} to Mn^{3+} ions in the mixed valence phase of Mn, leading to reduced double-exchange interaction (Mn^{3+}−O−Mn^{4+}) suppressing ferromagnetism. This loss of ferromagnetism results in reduced M_S and T_C (319.8 K) of the films. Also, the zero-field cooled (ZFC) and field-cooled (FC) magnetization curves start to separate from each other below T_C, which indicates that a weak antiferromagnetism or frustrated ferromagnetic phase begins to develop due to the surface treatments. Another interesting observation is reduced ferromagnetism in the sample where an AlO_x layer is inserted between the LSMO and rubrene molecule. In this case the direct contact between the d orbital of Mn and the π orbital of rubrene is intentionally restricted, and a decrease of both M_S and T_C is observed.

Also, the coercive fields (H_c) increase in all of the samples compared to pristine LSMO (0.5 mT). This increase in H_c is nearly 3 times that in the as-grown sample and nearly 5 times that in the vacuum-annealed one or in sample with an AlO_x layer. This indicates the formation of trapping/pinning sites for the magnetic domains at the interface that is formed due to coating of the rubrene molecules, where a higher external magnetic field is only able to switch the magnetization direction of LSMO. Additional trapping sites at the hybrid interface due to vacuum treatment of LSMO and the presence of Al can increase the coercive fields even further.

For an in-depth knowledge of the modified magnetic phase at the LSMO/rubrene interface, the relative change in magnetization ($\Delta M/M$) is calculated using the formula $[(M - M_{LSMO})/M_{LSMO}]$ and plotted as a function of temperature for samples A, B, and C in Figure 9a. For all of the samples the

DOI: 10.1021/acsami.5b04840
ACS Appl. Mater. Interfaces 2015, 7, 22228−22237

maximal change is observed near the Curie temperature T_C. $\Delta M/M$ decreases with decreasing temperature and eventually reaches a saturation value below 100 K. For sample A, the $\Delta M/M$ is positive, whereas for samples B and C its value is negative. Sample C shows a larger negative saturation ($\Delta M/M$) value (nearly −13%) with a sharper transition compared to sample B and sample A reaching a saturation value below 300 K. This indicates that due to direct chemical bonding between the LSMO and the organic molecule, redistribution of electronic charges across the interface causes some defect sites, making the transition from paramagnetic to ferromagnetic phase rather gradual. This hypothesis is also justified by the increased H_c values observed for these samples. Also, on vacuum-treated LSMO surfaces, oxygen vacancy related defects can hamper sharp switching to long-range FM ordering and cause decreased magnetization compared to pristine LSMO. Separation between ZFC and FC branches of magnetization for sample B also verifies that created defects or anti-ferromagnetic domains are present in them, which upon field cooling transforms into FM domains causing the observed pattern. For sample C, where rubrene was grown on AlO_x the PM-FM switching is much sharper, indicating fewer defect states at the interface, which is also supported by XRR data and earlier works in which the authors reported better growth of rubrene on AlO_x.[6] Also, it can be noted that after removal of rubrene molecules, the improved ferromagnetic property of LSMO surface still exists as shown in Figure 9b, although the M_S value decreases to 5.727 μ_B/fu. This indicates that there are two contributions present simultaneously. First, the rubrene molecule is chemically absorbed on the LSMO surface and changes its electronic and magnetic properties permanently, which was also observed for other organic materials.[37−39] Second, in close contact with ferromagnetic LSMO, a magnetic moment is induced in rubrene molecules that increases the saturation moment of the LSMO/rubrene sample. After removal of the rubrene layer from the LSMO surface, the real effect at the modified interface can be seen. It is clear that the saturation moment of LSMO is increased by 0.592 μ_B/fu considering the entire 20 nm thickness of LSMO. Because the main change is taking place in the top 1 nm layer (~2−3 unit cells) of the LSMO, the change in magnetization in the first 1 nm thickness of the film is 11.84 μ_B/fu, and the improvement in surface magnetization of LSMO is >230%.

This experimental observation of greatly modified magnetic property at the hybrid LSMO/organic interface is of major importance for the spintronics community. It has been already shown theoretically that the spin-resolved local density of states at the interface between a ferromagnet Fe and benzene molecule is modified due to the hybridization between π (p_z) orbitals of organic molecules and the d orbitals of the ferromagnet.[40] It was also shown that out-of plane spin d states of the clean ferromagnetic surface atoms are strongly modified under the organic molecules as a result of the hybridization. Said et al.[36] showed that this p-d hybridization and charge transfer strongly depend on the position of the aromatic molecule surface on the ferromagnetic interface. Therefore, we can conclude that by the different growth techniques of organic molecules it is possible to significantly modify the magnetic properties and hence the spin polarization of the hybrid interfaces. Insertion of AlO_x layer restricts this p-d hybridization and at the same time creates a modified band structure of LSMO. Rizwan et al.[41] have shown that the complex band structure of the amorphous insulating AlO_x temporarily modifies the majority and minority band edges. This modified band structure can lead to decreased ferromagnetism at the LSMO/AlO_x interface. Earlier, Yamada et al.[42] showed that ferromagnetic properties are strongly suppressed at the insulating oxide STO and LSMO interface. In the absence of any d elements in AlO_x, the bonding at this interface is predominantly of the sp-d character, which is expected to lead to less ferromagnetism suppression at the LSMO/ALO interface compared to that of LSMO/STO. Indeed, that is something we also observe experimentally. Whereas Yamada et al. reported strong suppression of T_C at the LSMO/STO interface, we observe a nearly 7% reduction in M_S and slightly decreased T_C at the LSMO/AlO_x interface.

Therefore, we can conclude that using pulsed laser deposition, it is possible to fabricate well-controlled interfaces with fewer defects for the hybrid spintronics devices. Further optimization of the growth parameters can lead to more improved molecular arrangements of organic semiconductors, leading to more versatile transport and magnetic properties of the spintronics components. Sensitive balance of molecular orientation at the FM-OS interface and better growth due to insertion of the tunnel barrier layer should be more carefully studied for confirming the p-d hybridization in the optimally functional devices.

CONCLUSION

We have demonstrated that a continuous, contamination-free hybrid inorganic ferromagnet/organic semiconductor interface can be fabricated using pulsed laser deposition techniques. Study of electronic properties and magnetic properties at the hybrid interface reveals the signature of hybridization of p orbitals of organic molecule and d electrons of the inorganic ferromagnet, which takes place at the interface leading to modified ferromagnetic properties of LSMO. The surface modification of ferromagnetic properties of LSMO leads to a change in saturation magnetic moment exceeding 230% and an increase in Curie temperature by 11 K in contact with the rubrene molecule. Intentional disruption of direct contact between LSMO and rubrene by insertion of a dielectric AlO_x layer leads to suppressed ferromagnetism of the hybrid interface. Previous ab initio calculation indicated that the position and orientation of the organic molecule on the ferromagnetic surface can substantially influence the interface magnetic properties, and together with the present results we can conclude that PLD can be used to grow different hybrid interfaces with substantial flexibility for designing the desired spin polarization properties. This result is of significance for artificial engineering of a highly spin polarized interface for future spintronics devices.

AUTHOR INFORMATION

Corresponding Author

*(S.M.) E-mail: sayani.majumdar@aalto.fi.

Author Contributions

The work was planned by S.M., who also performed XRD, XRR measurements and analysis, and magnetization data analysis and wrote the manuscript. K.G., M.S., and G.S. prepared the samples and took Raman measurements and data analysis. H.H. made magnetic measurements. J.D., M.T., and P.L. took XPS measurements and analyzed data. H.S.M. performed transport measurements and analysis. The manuscript was written

DOI: 10.1021/acsami.5b04840
ACS Appl. Mater. Interfaces 2015, 7, 22228−22237

through contributions of all authors. All authors have given approval to the final version of the manuscript.

Funding

COST Action MP1202 HINT, Kone Foundation Academy of Finland.

Notes

The authors declare no competing financial interest.

■ ACKNOWLEDGMENTS

We appreciate COST Action MP1202 HINT for inspiration and financial support. S.M. acknowledges the Kone Foundation and the Academy of Finland (Project 13293916) for financial support. K.G. acknowledges the National Science Centre of Poland (NCN) for financial support under Contract 2012/07/N/ST5/02139.

■ REFERENCES

(1) Dediu, V.; Hueso, L. E.; Bergenti, I.; Taliani, C. Spin Routes in Organic Semiconductors. *Nat. Mater.* **2009**, *8*, 707−716.
(2) Majumdar, S.; Majumdar, H. S.; Österbacka, R. Organic Spintronics. *Comprehensive Nanoscience and Technology*; Oxford Academic Press: New York, 2011; Vol. 1, pp 109−142.
(3) Sanvito, S. Molecular Spintronics. *Chem. Soc. Rev.* **2011**, *40*, 3336−3355.
(4) Sun, D.; Ehrenfreund, E.; Valy Vardeny, Z. The First Decade of Organic Spintronics Research. *Chem. Commun.* **2014**, *50*, 1781−1793.
(5) Park, J.-H.; Vescovo, E.; Kim, H.-J.; Kwon, C.; Ramesh, R.; Venkatesan, T. Direct Evidence for a Half-Metallic Ferromagnet. *Nature* **1998**, *392*, 794−796.
(6) Santos, T. S.; Lee, J. S.; Migdal, P.; Lekshmi, I. C.; Satpati, B.; Moodera, J. S. Room-Temperature Tunnel Magnetoresistance and Spin-Polarized Tunneling through an Organic Semiconductor Barrier. *Phys. Rev. Lett.* **2007**, *98*, 016601-1−4.
(7) Drew, A. J.; Hoppler, J.; Schulz, L.; Pratt, F. L.; Desai, P.; Shakya, P.; Kreouzis, T.; Gillin, W. P.; Suter, A.; Morley, N. A.; Malik, V. K.; Dubroka, A.; Kim, K. W.; Bouyanfif, H.; Bourqui, F.; Bernhard, C.; Scheuermann, R.; Nieuwenhuys, G. J.; Prokscha, T.; Morenzoni, E. Direct Measurement of the Electronic Spin Diffusion Length in a Fully Functional Organic Spin Valve by Low-Energy Muon Spin Rotation. *Nat. Mater.* **2009**, *8*, 109−114.
(8) Morley, N.; Rao, A.; Dhandapani, D.; Gibbs, M. R. J.; Grell, M.; Richardson, T. Room Temperature Organic Spintronics. *J. Appl. Phys.* **2007**, *103*, 07F306-1−3.
(9) Majumdar, S.; Majumdar, H. S. On the Origin of Decay of Spin Current with Temperature in Organic Spintronic Devices. *Org. Electron.* **2012**, *13*, 2653−2658.
(10) Majumdar, S.; Majumdar, H. S. Decay in Spin Diffusion Length with Temperature in Organic Semiconductors − an Insight of Possible Mechanisms. *Synth. Met.* **2013**, *173*, 26−30.
(11) Bergenti, I.; Dediu, V.; Prezioso, M.; Riminucci, A. Organic Spintronics. *Philos. Trans. R. Soc., A* **2011**, *369*, 3054−3068.
(12) Barraud, C.; Seneor, P.; Mattana, R.; Fusil, S.; Bouzehouane, K.; Deranlot, C.; Graziosi, P.; Hueso, L.; Bergenti, I.; Dediu, V.; Petroff, F.; Fert, A. Unravelling the Role of the Interface for Spin Injection into Organic Semiconductors. *Nat. Phys.* **2010**, *6*, 615−620.
(13) Morley, N.; Drew, A. J.; Zhang, H.; Scott, K.; Hudziak, S.; Morgan, D. J. Study of the Magnetic − Alq_3 Interface in Organic Spin-Valves. *Appl. Surf. Sci.* **2014**, *313*, 850−857.
(14) Djeghloul, F.; Ibrahim, F.; Cantoni, M.; Bowen, M.; Joly, L.; Boukari, S.; Ohresser, P.; Bertran, F.; Le Fèvre, P.; Thakur, P.; Scheurer, F.; Miyamachi, T.; Mattana, R.; Seneor, P.; Jaafar, A.; Rinaldi, C.; Javaid, S.; Arabski, J.; Kappler, J. − P.; Wulfhekel, W.; Brookes, N. B.; Bertacco, R.; Taleb-Ibrahimi, A.; Alouani, M.; Beaurepaire, E.; Weber, W. Direct Observation of a Highly Spin-Polarized Organic Spinterface at Room Temperature. *Sci. Rep.* **2013**, *3*, 1272−1−7.
(15) Grobosch, M.; Knupfer, M. Electronic Properties of Organic Semiconductor/Electrode Interfaces: The Influence of Contact Contaminations on the Interface Energetic. *Open Appl. Phys. J.* **2011**, *4*, 8−18.
(16) Białous, A.; Gazda, M.; Śliwiński, G. Structure and Optical Properties of TiO_2 Thin Films Prepared by Pulsed Laser Deposition. *Proc. SPIE* **2012**, *8770*, 877008-1−8.
(17) Grochowska, K.; Siuzdak, K.; Atanasov, P. A.; Bittencourt, C.; Dikovska, A.; Nedyalkov, N. N.; Śliwiński, G. Properties of Plasmonic Arrays Produced by Pulsed-Laser Nanostructuring of Thin Au Films. *Beilstein J. Nanotechnol.* **2014**, *5*, 2102−2112.
(18) Blanchet, G. B.; Fincher, C. R.; Malajovich, I. Laser Evaporation and the Production of Pentacene Films. *J. Appl. Phys.* **2003**, *94*, 6181−6184.
(19) Salih, A. J.; Lau, S. P.; Marshall, J. M.; Maud, J. M.; Bowen, W. R.; Hilal, N.; Lovitt, R. W.; Williams, P. M. Improved Thin Films of Pentacene via Pulsed Laser Deposition at Elevated Substrate Temperatures. *Appl. Phys. Lett.* **1996**, *69*, 2231−2233.
(20) Chrisey, D. B.; Hubler, G. K. Laser Deposition of Polymer and Biomaterial Films. *Chem. Rev.* **2003**, *103*, 553−576.
(21) Itaka, K.; Hayakawa, T.; Yamaguchi, J.; Koinuma, H. Pulsed Laser Deposition of c* Axis Oriented Pentacene Films. *Appl. Phys. A: Mater. Sci. Process.* **2004**, *79*, 875−877.
(22) Salih, A. J.; Marshall, J. M. High-Mobility Low-Threshold-Voltage Pentacene Thin-Film Transistors Prepared at Rapid Growth Rates by Pulsed-Laser Deposition. *Philos. Mag. Lett.* **1997**, *75*, 169−177.
(23) Yamaguchi, J.; Itaka, K.; Hayakawa, T.; Arai, K.; Yamashiro, M.; Yaginuma, S.; Koinuma, H. Combinatorial Pulsed Laser Deposition of Pentacene Films for Field Effect Devices. *Macromol. Rapid Commun.* **2004**, *25*, 334−338.
(24) Grochowska, K.; Majumdar, S.; Laukkanen, P.; Majumdar, H. S.; Sawczak, M.; Śliwiński, G. Pulsed Laser Deposition of Organic Semiconductor Rubrene Thin Films. *Proc. SPIE* **2014**, *9447*, 94470F-1−7.
(25) Majumdar, S.; van Dijken, S. Pulsed Laser Deposition of $La_{1-x}Sr_xMnO_3$: Thin-Film Properties and Spintronic Applications. *J. Phys. D: Appl. Phys.* **2014**, *47*, 03410−1−15.
(26) Wang, L. D.; Kwok, H. S. Pulsed Laser Deposition of Organic Thin Films. *Thin Solid Films* **2000**, *363*, 58−60.
(27) Yao, L.; Majumdar, S.; Äkäslompolo, L.; Inkinen, S.; Qin, Q. H.; van Dijken, S. Electron-Beam-Induced Perovskite−Brownmillerite−Perovskite Structural Phase Transitions in Epitaxial $La_{2/3}$ $Sr_{1/3}MnO_3$ Films. *Adv. Mater.* **2014**, *26*, 2789−2793.
(28) Weinberg-Wolf, J. R.; McNeil, L. E.; Liu, S.; Kloc, C. Evidence of Low Intermolecular Coupling in rubrene Single Crystals by Raman Spectroscopy; http://research.physics.unc.edu/project/mcneil/MolecularAnimations/anim.php.
(29) Henn, D. E.; Williams, W. G.; Gibbons, D. J. Crystallographic Data for an Orthorhombic Form of Rubrene. *J. Appl. Crystallogr.* **1971**, *4*, 256.
(30) Majumdar, S.; Kooser, K.; Elovaara, T.; Huhtinen, H.; Granroth, S.; Paturi, P. Analysis of Electronic Structure and its Effect on Magnetic Properties in (001) and (110) Oriented $La_{0.7}Sr_{0.3}MnO_3$ Thin Films. *J. Phys.: Condens. Matter* **2013**, *25*, 376003-1−9.
(31) Han, S. W.; Lee, J. D.; Kim, K. H.; Song, H.; Kim, W. J.; Kwon, S. J.; Lee, H. G.; Hwang, C.; Jeong, J. I.; Kang, J.-S. Electronic Structures of the CMR Perovskites $R_{1-x}A_xMnO_3$ (R = La, Pr; A = Ca, Sr, Ce) Using Photoelectron Spectroscopy. *J. Korean Phys. Soc.* **2002**, *40*, 501−510.
(32) Hishida, T.; Ohbayashi, K.; Kobata, M.; Ikenaga, E.; Sugiyama, T.; Kobayashi, K.; Okawa, M.; Saitoh, T. Empirical Relationship Between X-ray Photoemission Spectra and Electrical Conductivity in a Colossal Magnetoresistive Manganite $La_{1-x}Sr_xMnO_3$. *J. Appl. Phys.* **2013**, *113*, 233702-1−4.
(33) Saeki, A.; Seki, S.; Takenobu, T.; Iwasa, Y.; Tagawa, S. Mobility and Dynamics of Charge Carriers in rubrene Single Crystals Studied by Flash-Photolysis Microwave Conductivity and Optical Spectroscopy. *Adv. Mater.* **2008**, *20*, 920−923.

DOI: 10.1021/acsami.5b04840
ACS Appl. Mater. Interfaces 2015, 7, 22228−22237

(34) Seo, S.; Park, B. − N.; Evans, P. G. Ambipolar Rubrene Thin Film Transistors. *Appl. Phys. Lett.* **2006**, *88*, 232114-1−3.
(35) Garcia, V.; Bibes, M.; Barthélémy, A.; Bowen, M.; Jacquet, E.; Contour, J.-P.; Fert, A. Temperature Dependence of the Interfacial Spin Polarization of $La_{2/3}Sr_{1/3}MnO_3$. *Phys. Rev. B: Condens. Matter Mater. Phys.* **2004**, *69*, 052403-1−4.
(36) Goumri-Said, S.; Kanoun, M. B.; Manchon, A.; Schwingenschlögl, U. Spin-Polarization Reversal at the Interface Between Benzene and Fe (100). *J. Appl. Phys.* **2013**, *113*, 013905-1−4.
(37) Majumdar, S.; Dey, S.; Huhtinen, H.; Dahl, J.; Tuominen, M.; Laukkanen, P.; van Dijken, S.; Majumdar, H. S. Comparison of Spin Response in Alq3 and Co-Pthalocyanine Based Organic Spin Valves. *SPIN* **2014**, *4*, 1440009-1−12.
(38) Pesonen, M.; Majumdar, S.; Huhtinen, H.; Paturi, P.; Majumdar, H. S.; Österbacka, R. Effects of Conjugated Polymer on the Magnetotransport Properties in $La_{0.7}Sr_{0.3}MnO_3$ Ferromagnetic Electrodes. *AIP Adv.* **2013**, *3*, 042102-1−8.
(39) Majumdar, S.; Laiho, R.; Laukkanen, P.; Värynen, J.; Majumdar, H. S.; Österbacka, R. Application of Regioregular Polythiophene in Spintronic Devices: Effect of Interface. *Appl. Phys. Lett.* **2006**, *89*, 122114-1−3.
(40) Atodiresei, N.; Brede, J.; Lazić, P.; Caciuc, V.; Hoffmann, G.; Wiesendanger, R.; Blügel, S. Design of the Local Spin Polarization at the Organic-Ferromagnetic Interface. *Phys. Rev. Lett.* **2010**, *105*, 066601-1−4.
(41) Rizwan, S.; Guo, S. M.; Wang, Y.; Wen, Z. C.; Zhang, S.; Zhao, Y. G.; Zou, J.; Han, X. F. Temperature and Bias-Assisted Transport Properties of LSMO/AlO/CoFeB Magnetic Tunnel Junction. *IEEE Trans. Magn.* **2010**, *46*, 2383−2386.
(42) Yamada, H.; Ogawa, Y.; Ishii, Y.; Sato, H.; Kawasaki, M.; Akoh, H.; Tokura, Y. Engineered Interface of Magnetic Oxides. *Science* **2004**, *305*, 646−648.

DOI: 10.1021/acsami.5b04840
ACS Appl. Mater. Interfaces 2015, 7, 22228−22237